

## Identification of metal compounds in alum-treated wood from the Oseberg collection

Caitlin M. A. McQueen<sup>1,\*</sup>, Diego Tamburini<sup>2,a</sup> and Susan Braovac<sup>1</sup>

(1) Museum of Cultural History, University of Oslo, Postboks 6762 St. Olavs plass, 0130 Oslo, Norway

(2) Department of Chemistry and Industrial Chemistry, University of Pisa, via Moruzzi 13, I-56124 Pisa, Italy

\*E-mail: caitlin.mcqueen@khm.uio.no

### Abstract

Wooden artefacts from the Oseberg collection contain various metal compounds arising from factors such as alum-treatment, the use of metal joiners and storage in metal tanks. Such compounds can significantly influence the condition of the wood, and therefore inorganic characterisation is important to include in studies of the wood. Using XRD, FTIR spectroscopy and SEM-EDS, we have been able to characterise metal compounds in several alum-treated wood fragments, including alum decomposition products, iron and zinc corrosion products and combinations thereof.

### Keywords

alum, archaeological wood, iron corrosion, XRD, IR, SEM-EDS

### Introduction

Artefacts from the Oseberg burial, housed at the Viking Ship Museum in Oslo, Norway, represent one of the most comprehensive collections of Viking Age wooden objects in the world. Upon excavation in the early 1900s, the objects were treated and reconstructed using a variety of materials. Apart from the alum ( $\text{KAl}(\text{SO}_4)_2 \cdot 12\text{H}_2\text{O}$ ) used to conserve the more deteriorated waterlogged wood, the objects were treated and restored using metal nails and screws, glues, putties, linseed oil and varnishes. The resulting objects contain a significant non-wood component, including various metal compounds.

More recently it has become clear that the alum treatment applied to many waterlogged wooden objects in the past was ultimately very damaging, leading to high acidity and loss of structural integrity (Christensen 1970, Hoffmann et al. 2002, Häggström et al. 2013, Braovac 2015). This is due in no small part to the release of sulfuric acid ensuing from hydrolysis of alum during treatment (Braovac and Kutzke 2012). Pyrolysis-gas chromatography/mass spectrometry (Py-GC/MS) and Fourier transform infrared (FTIR) analyses of a series of alum-treated fragments from the Oseberg collection revealed extreme depletion of holocellulose and oxidation of lignin, and corresponding results of inductively coupled plasma atomic emission spectroscopy (ICP-AES) have suggested that the wood degradation was higher where alum concentration was higher and that iron ions could be accelerating the degradation of the wood (Braovac 2015, Braovac et al. 2016, McQueen et al. 2017).

The detrimental effect of iron ions on archaeological wood has been the subject of several studies (MacLeod et al. 1990, Almkvist and Persson 2008, Wetherall et al. 2008, Almkvist and Persson 2011, Norbakhsh et al. 2013, Norbakhsh et al. 2014). However, the concentration

---

<sup>a</sup> Present address: Department of Scientific Research, The British Museum, Great Russell Street, London WC1B 3DG

of iron found in the series' from the Oseberg collection is generally significantly lower (<0.2% w/w) than those considered in the previous studies, and these early observations highlight the fact that relatively low concentrations of iron might still significantly influence the condition of the wood. This is perhaps unsurprising given that iron ions are believed to play a catalytic role in wood degradation (Emery and Schroeder 1974, Henry 2003). Furthermore, the previous work on iron in archaeological wood has focused on artefacts from marine environments, in which the combination of corroding iron and products from sulfate reducing bacteria had resulted in accumulation of iron sulfides that began to oxidise after excavation.

Most of the artefacts in these previous reports were treated with polyethylene glycol, rather than alum as in the Oseberg collection. Though dire consequences of the alum treatment, such as compromised structural integrity and extreme deterioration of wood polymers, are now being observed, these are not yet well understood. The chemistry and reactivity of alum is a key matter in any examination of metal compounds contained in these objects. Other inorganic components add further complexity.

The previous ICP-AES analyses disclosed the presence of a range of metallic elements, but identification of the compounds these comprise requires other analytical techniques. Such information could provide important insight into chemical processes occurring in these vulnerable objects. We herein describe some early results of inorganic characterisation in several fragments from Oseberg artefacts.

## **Materials and methods**

### *Samples*

Samples were collected from ten uncoated alum-treated fragments from two separate objects. Six fragments, are thought to have originally fit together in a weaving loom, object 185, and are numbered 185-1 to 185-6 (Figure 1a). The other four fragments are from a simple sled, object 229, and are labelled Fragments 1B-D and 5 (Figure 1b). Details of a range of organic, inorganic and morphological analysis on samples from these fragments have now been published (Braovac 2015, Braovac et al. 2016, McQueen et al. 2017).

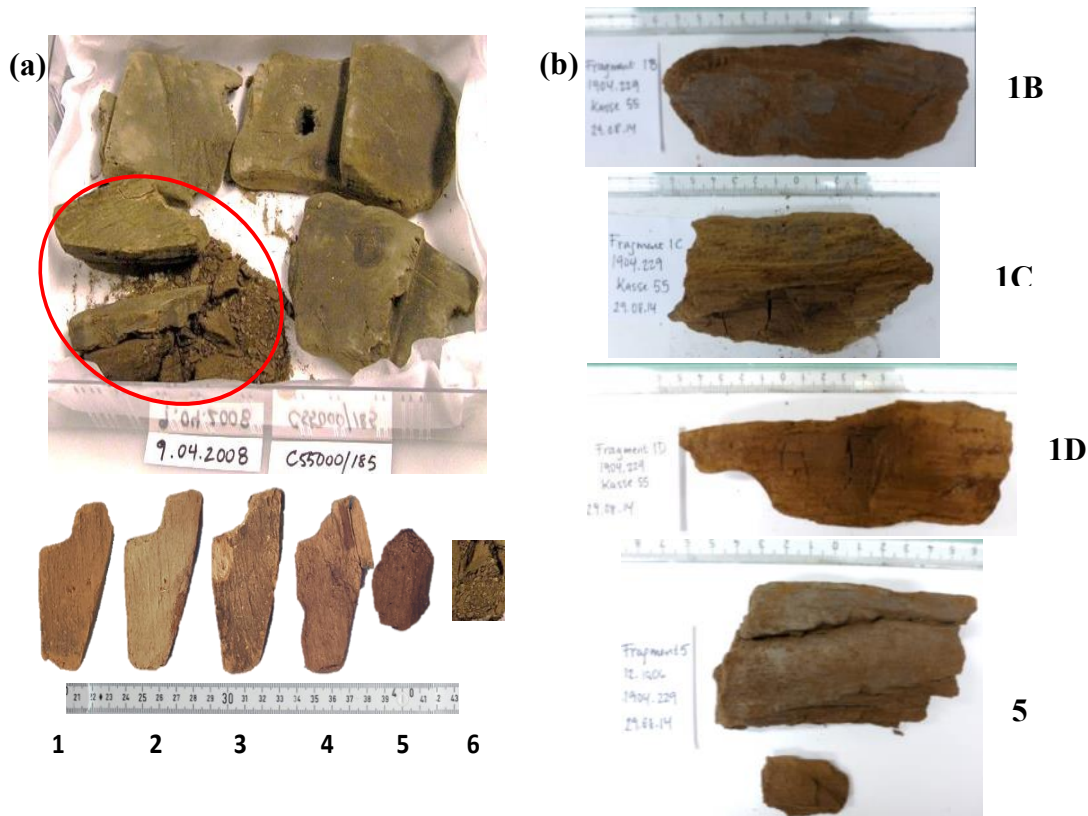


Figure 1. Fragments of uncoated, alum-treated wood from the Oseberg collection from which samples were collected: (a) 185 fragments 1-6; (b) 229 fragments 1B, 1C, 1D and 5.

Samples were also collected from a fragment of object 195, a sled. The fragment is an uncoated alum-treated piece which has broken into three pieces to reveal an iron rod that was introduced during reconstruction in the early 1900s. A sample of the powdery corrosion layer was taken (195A). Wood samples were also taken from the inner surface of the smallest fragment, both underneath the corrosion layer (195B) and toward the edge further away from where the rod would have sat (195C), as indicated in Figure 2. The powdery corrosion product was brushed from the surface of the wood before taking these samples.



Figure 2. Object 195 with sampling areas 195A-C indicated.

### *FTIR spectroscopy*

FTIR spectra in attenuated total reflection (ATR) mode were recorded on a Thermo Scientific Nicolet iS50 spectrometer equipped with a diamond crystal and DTGS detector. Spectra were recorded with 32 scans at  $4\text{ cm}^{-1}$  resolution, within the range  $4000\text{-}400\text{ cm}^{-1}$ .

Some spot analyses and mapping were performed both with conventional IR radiation (using the above instrument), and synchrotron radiation (SR). SR-FTIR, which gave improved spatial resolution, was carried out at the IRIS beamline at the BESSY II synchrotron facility, Helmholtz-Zentrum Berlin Germany, using a Nicolet Nexus 870 spectrometer. Samples were compressed in a diamond cell and micro-infrared spectroscopy ( $\mu$ FTIR) performed using a Nicolet Continuum FTIR microscope. Spectra were recorded in transmittance mode with a spectral resolution of  $4\text{ cm}^{-1}$ , within the range  $4000\text{-}650\text{ cm}^{-1}$  and  $4000\text{-}800\text{ cm}^{-1}$  for conventional and synchrotron radiation, respectively. Each spectrum in the maps was recorded with 128 scans and spot analyses were recorded with 256 scans.

### *XRD*

X-ray diffraction analysis was carried out using a PANalytical diffractometer Empyrean Series 2 with radiation  $\text{CuK}\alpha 1 = 1.54\text{ \AA}$ , operating at 45 kV, 40 mA,  $2\theta$  range  $8\text{-}70^\circ$ , step size  $0.03^\circ$ , time per step 5000 s, equipped with a PIXcel<sup>1D</sup>-Medipix3 RTMS detector, and High Score data acquisition and interpretation software. A zero background sample holder was used. Crystalline phases were identified using the ICDD database.

### *SEM-EDS*

Analyses were performed using a FEI Quanta 450 Scanning Electron Microscope coupled with an Oxford X-Max<sup>N</sup> 50mm<sup>2</sup> detector, using low vacuum mode to avoid charging and a voltage of 20 kV. The other parameters (spot size, pressure, and working distance) were modified depending on the sample.

## **Results and discussion**

### *Hydrolysis of alum*

The acidity of the alum treatment arises from hydrolysis reactions that occur in solution. From previous reports we can summarise the relevant reactions in equations (1) and (2) (Braovac and Kutzke 2012, Braovac 2016, McQueen et al. 2017).



At room temperature (1), alum can undergo hydrolysis to give acidic solutions. The objects, however, were treated at  $90^\circ\text{C}$ , and the formation of white precipitate was observed. Later experiments showed that this contained alunite ( $\text{KAl}_3(\text{SO}_4)_2(\text{OH})_6$ ) (Braovac and Kutzke 2012). Alunite is insoluble in water and readily precipitates, removing it from the solution and driving the reaction to the right, leaving dissolved potassium, sulfate and hydronium ions to be absorbed into the wood.

Alunite was not identified in any of the samples from objects 185, 229 or 195. However, other by-products of these reactions were found. Mercurite ( $\text{KHSO}_4$ ) was identified in almost all of the fragments from 185 and 229 either by XRD or FTIR microscopy (McQueen et al. 2017) (Figure 3). The relative abundance of mercurite to alum was higher in the most alum-poor samples, from the inner regions of 229-1C and 229-1D, than in any of the other samples, indicating that it had migrated into the wood more readily than alum.

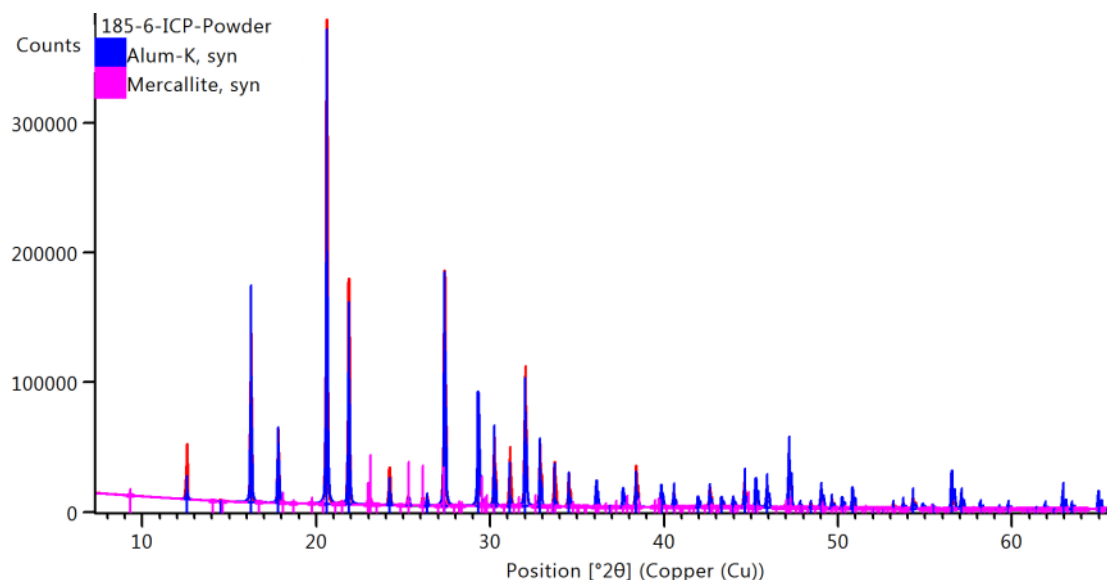


Figure 3. X-ray diffraction pattern for sample 185-6 showing major peaks from alum and minor peaks from mercurite.

#### *Iron corrosion in alum-treated wood*

The corroding rod in 195 was confirmed as iron by SEM-EDS. The presence of the thick powdery layer of corrosion product is unsurprising, given that an acidic environment such as alum-treated wood should accelerate the oxidation of iron. Accordingly, a pH of 2 was measured on the wood surface (taken close to sampling area 195C with an indicator strip).

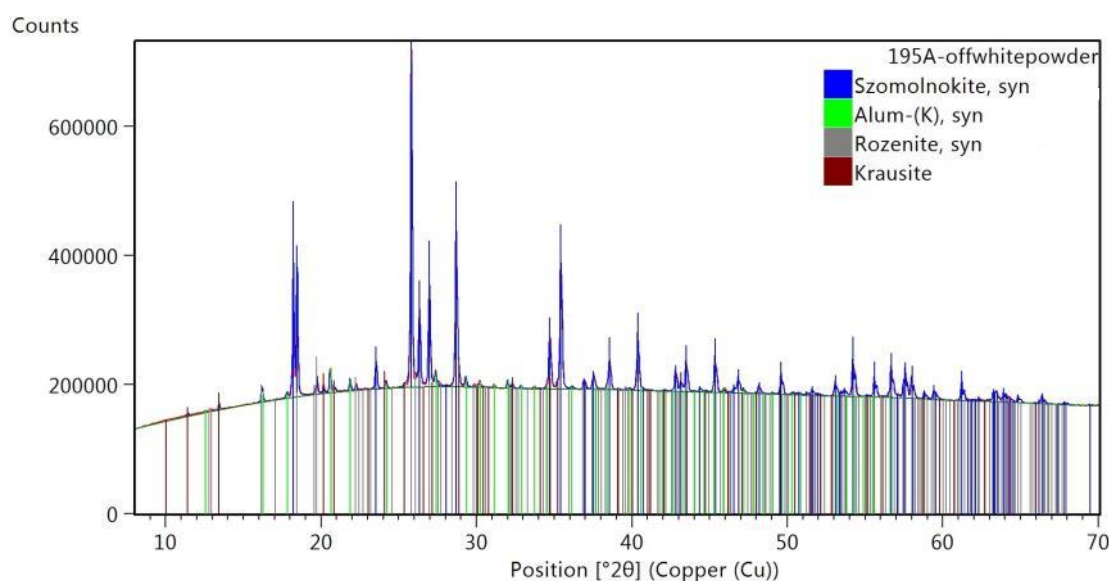


Figure 4. XRD pattern of 195A showing major peaks from szomolnokite ( $\text{FeSO}_4 \cdot \text{H}_2\text{O}$ ) and minor peaks from rozenite ( $\text{FeSO}_4 \cdot 4\text{H}_2\text{O}$ ) and krausite ( $\text{KFe}(\text{SO}_4)_2 \cdot \text{H}_2\text{O}$ ) in addition to alum.

The XRD pattern of the off-white powder, 195A (Figure 4), on the iron rod suggested the major component was the iron(II) sulfate mineral szomolnokite ( $\text{FeSO}_4 \cdot \text{H}_2\text{O}$ ). This was confirmed by ATR-FTIR spectroscopy. This compound was found in smaller proportions in the two wood samples, 195B (Figure 5) and 195C (Figure 7) by XRD, as well as by FTIR microscopy in 195B (Figure 6). Another form of iron(II) sulfate, rozenite ( $\text{FeSO}_4 \cdot 4\text{H}_2\text{O}$ ) was also found in 195A. Evidence that this corrosion product undergoes further oxidation and reactions with alum is seen in the form of potassium iron(III) sulfate minerals. Either krausite or goldichite ( $\text{KFe}(\text{SO}_4)_2 \cdot \text{H}_2\text{O}$  and  $\text{KFe}(\text{SO}_4)_2 \cdot 4\text{H}_2\text{O}$ , respectively), were identified in all samples in this fragment. SEM-EDS phase analyses also supported the presence of iron sulfate and potassium iron sulfate in 195B and 195C.

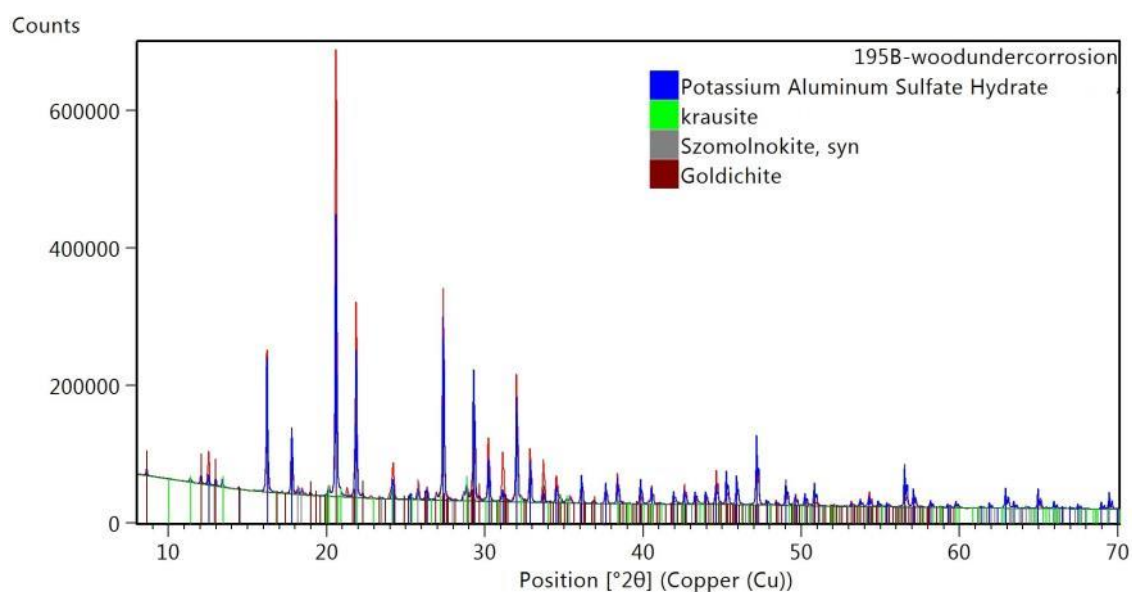


Figure 5. XRD pattern of 195B showing major peaks from alum and minor peaks from krausite ( $\text{KFe}(\text{SO}_4)_2 \cdot \text{H}_2\text{O}$ ), szomolnokite ( $\text{FeSO}_4 \cdot \text{H}_2\text{O}$ ) and goldichite ( $\text{KFe}(\text{SO}_4)_2 \cdot 4\text{H}_2\text{O}$ ).

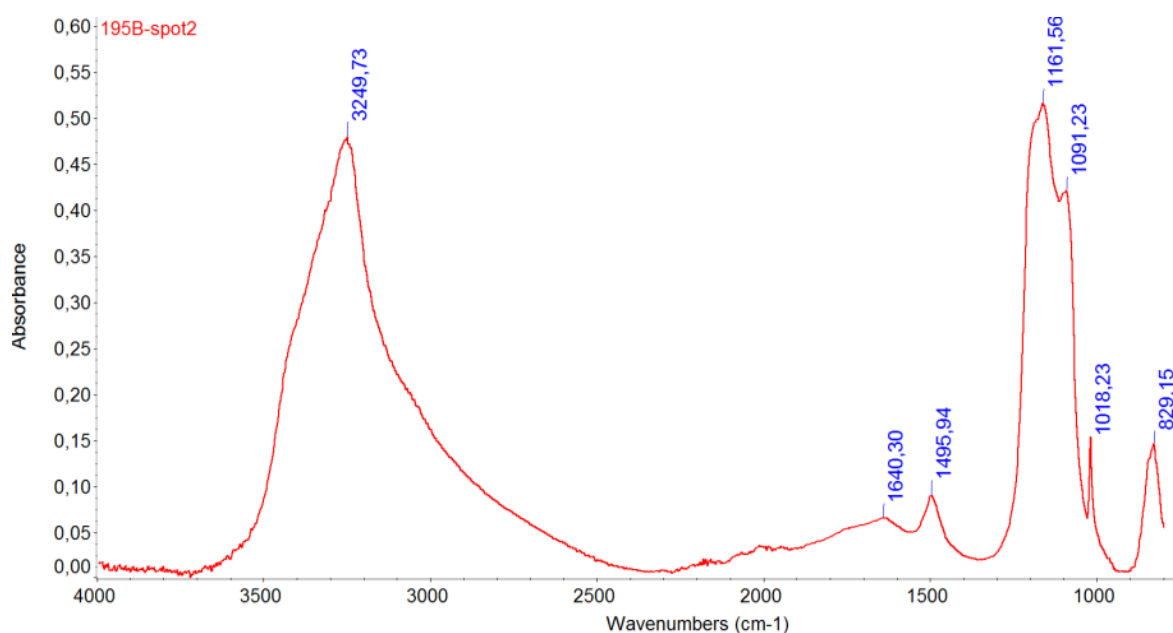


Figure 6. SR  $\mu$ -FTIR spectra from sample 195B showing peaks similar to literature peaks for szomolnokite (Chukanov 2014).

## Zinc compounds

Though there were several minor compounds evident in the complex diffraction patterns of 195B and 195C, mercurite could not be recognised among them. Though many of these minor peaks remain unidentified, some in the XRD pattern of 195C matched those of a potassium zinc sulfate compound ( $K_2(Zn(H_2O)_6)(SO_4)_2$ ) (Figure 7). Overlapping regions of K, Zn and S abundance seen by SEM-EDS (Figure 8) support the presence of this compound.

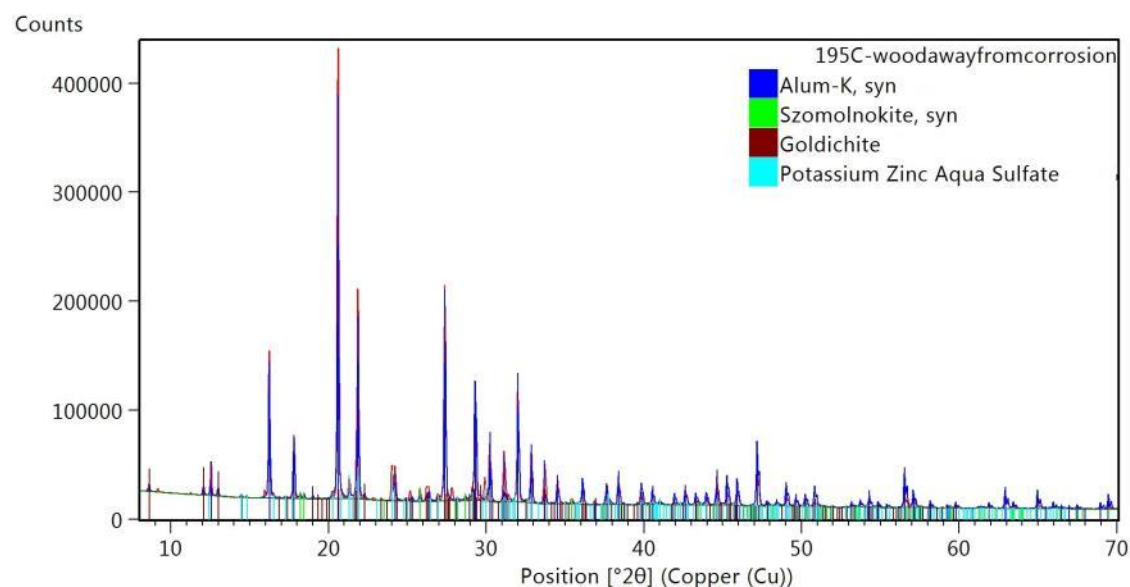


Figure 7. XRD pattern of 195C showing major peaks from alum and minor peaks from szomolnokite ( $FeSO_4 \cdot H_2O$ ), goldichite ( $KFe(SO_4)_2 \cdot 4H_2O$ ) and  $K_2(Zn(H_2O)_6)(SO_4)_2$ .

Fragments from 185 were also found to contain significant levels of zinc by ICP analyses, and this is thought to be due to storage in zinc tanks after excavation (Braovac et al. 2016). The sampling area of 195C is closest to what would have been the outer surface of the fragment (before further fragmentation), so the presence of the zinc compound here is consistent with zinc absorbed from a storage tank.

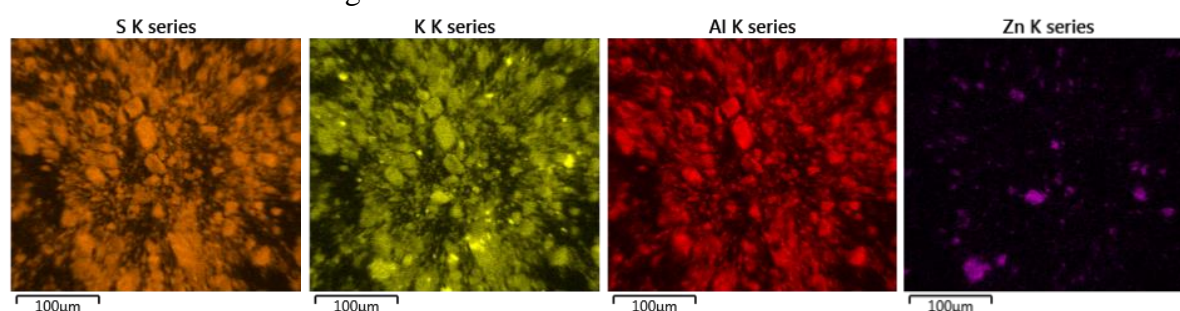


Figure 8. SEM-EDS elemental maps for 195C, showing areas of coinciding K, S and Zn abundance that do not coincide with Al, supporting the presence of a potassium zinc sulfate.

## Conclusions

The use of XRD, FTIR and SEM-EDS analysis has allowed identification of various metal compounds related to alum treatment, iron corrosion and storage conditions in wood samples from the Oseberg collection. XRD has been a particularly useful tool, identifying various crystalline inorganic compounds, often in mineralogical form.

The results have indicated that the hydrolysis of alum in solution has led to the deposition of mercurite in several treated wood fragments, which appears to migrate more readily into the inner regions than alum itself. A fragment containing an iron rod did not contain this product, but did display extensive corrosion of the rod and high acidity of the wood, resulting in the formation of iron(II) sulfates. These have reacted further with alum (or degradation products thereof) to form potassium iron(III) sulfate minerals.

Furthermore, storage of the objects in zinc tanks appears to have caused some absorption of zinc into the wood, which has undergone reactions with alum to form a detectable amount of a potassium zinc sulfate in one wood sample.

Further work is underway to characterize inorganic compounds in a larger variety of environments in alum-treated wood artefacts from the collection, and to investigate their effect on the extent of degradation of the wood.

### **Acknowledgements**

This work was carried out as part of the Saving Oseberg project, funded by the Norwegian Ministry of Education and University of Oslo. The authors wish to thank Helmholtz-Zentrum Berlin for the allocation of synchrotron beamtime for FTIR measurements. The assistance of Ulrich Schade and Ljiljana Puskar at the IRIS beamline is gratefully acknowledged. The authors would also like to thank Hartmut Kutzke for assistance with synchrotron beamtime and contributions to scientific discussions.

### **References**

- Almkvist, G. and I. Persson. 2008. Analysis of acids and degradation products related to iron and sulfur in the Swedish warship Vasa. *Holzforschung*, 62: 694-703.
- Almkvist, G. and I. Persson. 2011. Distribution of iron and sulfur and their speciation in relation to degradation processes in wood from the Swedish warship Vasa. *New Journal of Chemistry*, 35: 1491-1502.
- Braovac, S. 2015. Alum-treated wood material characterization: A case study of the Oseberg finds. PhD thesis, The Royal Danish Academy of Fine Arts, Schools of Architecture, Design and Conservation, Copenhagen.
- Braovac, S. and H. Kutzke. 2012. The presence of sulfuric acid in alum-conserved wood – Origin and consequences. *Journal of Cultural Heritage*, 13(3): S203-208.
- Braovac, S., D. Tamburini, J. J. Łucejko, C. McQueen, H. Kutzke, and M. P. Colombini. 2016. Chemical analyses of extremely degraded wood using analytical pyrolysis and inductively coupled plasma atomic emission spectroscopy. *Microchemical Journal*, 124: 368-379.
- Christensen, B. B. 1970. *The conservation of waterlogged wood in the National Museum of Denmark*. Copenhagen: The National Museum of Denmark.
- Chukanov, N. V. 2014. *Infrared spectra of mineral species: Extended library*. Dordrecht: Springer.

Emery, J. and H. Schroeder. 1974. Iron-catalyzed oxidation of wood carbohydrates. *Wood Science and Technology*, 8(2):123-137.

Henry, W. P. 2003. Non-enzymatic iron, manganese, and copper chemistry of potential importance in wood decay. In *Wood Deterioration and Preservation*, ed. B. Goodell, D. D. Nicholas and T. P. Schulz, 175-195. Washington, DC: American Chemical Society.

Hoffmann, P., E. Schwab, and N. Bonde. 2002. Report on strength tests performed on wood samples from the Gokstad Ship and boats, and from the Oseberg finds complex, and some observations on strakes from the Gokstad, Oseberg and Tune ships. In *Vikingskipsseminaret*, ed, A. Bøe, 71-85. Oslo: University of Oslo.

Häggström, C., K. Lindahl, M. Sahlstedt and T. Sandström. 2013. *Alum-treated archaeological wood: Characterization and re-conservation*. Stockholm: Swedish National Heritage Board.

MacLeod, I. D., P. Brooke, and V. Richards. 1990. Iron corrosion products and their interactions with waterlogged wood and PEG. In *Proceedings of the 4th ICOM-Group on Wet Organic Archaeological Materials Conference*, Bremerhaven, 1990, ed. P. Hoffmann, pp. 119-132. Bremerhaven: ICOM-CC WOAM.

McQueen, C. M. A., D. Tamburini, J. J. Łucejko, S. Braovac, F. Gambineri, F. Modugno, M. P. Colombini and H. Kutzke. 2017. New insights into the degradation processes and influence of the conservation treatment in alum-treated wood from the Oseberg collection. *Microchemical Journal*,. 132: 119-129.

Norbakhsh, S., I. Bjurhager, and G. Almkvist. 2013. Mimicking of the strength loss in the Vasa: model experiments with iron-impregnated recent oak. *Holzforschung*, 67(6): 707-714

Norbakhsh, S., I. Bjurhager, and G. Almkvist. 2014. Impact of iron (II) and oxygen on degradation of oak – Modeling of the Vasa wood. *Holzforschung*, 68(6): 649-655.

Wetherall, K. M., R. M. Moss, A. M. Jones, A. D. Smith, T. Skinner, D. M. Pickup, S. W. Goatham, A. V. Chadwick, and R. J. Newport. 2008. Sulfur and iron speciation in recently recovered timbers of the Mary Rose revealed via X-ray absorption spectroscopy. *Journal of Archaeological Science*, 35: 1317-1328.